Efficient synthesis, crystallography study, antibacterial/antifungal activities, DFT/ADMET studies and molecular docking of novel α-aminophosphonates

Rania Bahadi, Malika Berredjem, Chahrazed Benzaid, Fouzia Bouchareb, Ali Dekir, Manel Lina Djendi, Malika Ibrahim-Ouali, Meriem Boussaker, Sofiane Bouacida, Ajmal Rashid Bhat, et al.

Journal of Molecular Structure 1289 (2023) 135849

Contents lists available at ScienceDirect

Journal of Molecular Structure

journal homepage: www.elsevier.com/locate/molstr

Efficient synthesis, crystallography study, antibacterial/antifungal activities, DFT/ADMET studies and molecular docking of novel α-aminophosphonates

Rania Bahadi [a], Malika Berredjem [a,*], Chahrazed Benzaid [a], Fouzia Bouchareb [a,b], Ali Dekir [a], Manel Lina Djendi [a], Malika Ibrahim-Ouali [c], Meriem Boussaker [a], Sofiane Bouacida [d,e], Ajmal Rashid Bhat [f], Sumeer Ahmed [f,g], Khaldoun Bachari [h], Rayenne Redjemia [a]

[a] Laboratory of Applied Organic Chemistry, Synthesis of Biomolecules and Molecular Modelling Group, Department of Chemistry, Sciences Faculty, Badji-Mokhtar-Annaba University, Box 12, Annaba 23000, Algeria
[b] Department of Chemistry, Faculty of Sciences and Technology, Chadli Bendjedid EL-Tarf University, Box: 73, El-Tarf 36000, Algeria
[c] Aix Marseille Univ, CNRS, Centrale Marseille, iSm2, Marseille, France
[d] Département sciences de la matière, Université Oum El Bouaghi, Oum El Bouaghi 04000, Algérie
[e] Unité de Recherche de Chimie de l'Environnement et Moléculaire Structurale, Université Frères Mentouri Constantine, 25000, Algérie
[f] Department of Chemistry, RTM Nagpur University, Nagpur 440033, India
[g] Research Department of Chemistry, The New College (Autonomous), University of Madras, Chennai- 600 014, India
[h] Centre de Recherche Scientifique et Technique en Analyses Physico-chimiques (CRAPC), BP384, Bou-Ismail, RP 42004, Tipasa, Algeria.

ARTICLE INFO

Keywords:
A-aminophosphonates
RX study
Antibacterial activity
Antifungal activity
Molecular docking
Dft
ADMET

ABSTRACT

An efficient method for the synthesis of a new series of α-aminophosphonates has been developed in a one-pot Kabachnik-Fields reaction of 4-methylaminophenol with various aldehydes and triethylphosphite under microwave irradiation and neat conditions using ZnO nanoparticles as a reusable and heterogeneous catalyst, with 82–93% yield at 250 Hz within 2-5 min. A single crystal of the studied compound 3e was selected for X-ray diffraction analysis, it crystallizes in the monoclinic crystal system with P 21/n space group. All the compounds were evaluated for their antimicrobial against a panel of Gram-negative pathogenic bacteria such as *Escherichia coli, Klebsiella pneumoniae, Acinetobacter baumannii, Serratia marcescens, Morganella morganii, Pseudomonas aeruginosa and Gram-positive :Staphylococcus aureus* and against fungi : *Candida albicans, Candida krusei, Candida kefyr, Candida lusitaniae, and Candida tropicalis*. Further in silico target hunting reveals the antibacterial activity of the designed compounds by inhibiting Dihydropteroate synthase and all the designed compounds have shown significant drug-like characteristics.

1. Introduction

Organophosphorus constitutes a significant class of chemical substances that exhibit high levels of activity across diverse fields including industry, agriculture, and medicine [1]. In recent years, significant focus has been directed towards the synthesis of α-aminophosphonate esters 1 and α-aminophosphonic acids 2, which are recognized as analogs of amino acids 3 wherein the carboxylic group has been substituted with a phosphoric group Fig. 1.

The literature reports the biological properties of α-aminophosphonates, which have been found to exhibit diverse and significant activity such as anticancer [2], antibacterial [3], antitumor [4], anti-inflammatory, and antimicrobial effects [5] Fig. 2. Furthermore, these compounds are used as antifungal, antiviral agents [6,7] and herbicides [8,9]. For that reason, the synthesis of α-aminophosphonates has received considerable attention, and significant progress has been made to develop more efficient methods for the synthesis of these compounds; in the following, we briefly discuss some of them. In 1952 Martin Izrailevich Kabachnik and Ellis K. Fields had discovered a novel multicomponent reaction for the synthesis of α-aminophosphonate from an amine, a carbonyl compound and a dialkyl phosphate in the presence of a catalyst. The multicomponent reaction was named after them as Kabachnik-Field reaction [10]. The second pathway is the Pudovik reaction [11] where dialkyl phosphite or trialkyl phosphite is added to

* Corresponding author.
E-mail address: malika.berredjem@univ-annaba.org (M. Berredjem).

https://doi.org/10.1016/j.molstruc.2023.135849
Received 6 April 2023; Received in revised form 29 April 2023; Accepted 23 May 2023
Available online 27 May 2023

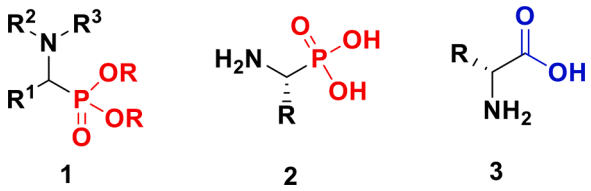

Fig. 1. Structures of α-aminophosphonate 1, α-aminophosphonic acids 2 and α-amino acids 3.

compounds containing imino bond in the presence of either base or Lewis catalyst. Another method for the synthesis of α-aminophosphonates is the use of the Mitsunobu reaction [12]. In this case, an hydroxyphosphonate is subjected to Mitsunobu reaction conditions with an amine.

Due to its importance, the synthesis of α-aminophosphonates has garnered considerable attention, prompting significant advancements towards the development of more efficient synthetic methodologies for these compounds. In the following, we will briefly discuss some of them; in 1952 Martin Izrailevich Kabachnik and Ellis K. Fields discovered a novel multicomponent reaction for the synthesis of α-aminophosphonate from an amine, a carbonyl compound, and a dialkyl phosphate in the presence of a catalyst. The multicomponent reaction was named after them as the Kabachnik- Field reaction [10]. The second pathway is the Pudovik reaction [11] where dialkyl phosphite or trialkyl phosphite are added to the compounds containing imino bonds in the presence of either base or Lewis catalyst. Another method for the synthesis of α-aminophosphonates is the use of the Mitsunobu reaction [12]. In this case, hydroxyphosphonate is subjected to Mitsunobu reaction condition with an amine.

In this context, and in connection with our green chemistry program, we recently reported an efficient and "one-pot" three-component procedure for the synthesis of new biologically actives α-aminophosphonates [13]. In this paper, the reactions were carried out by mixing the reagents (aldehyde, hydroxyaniline and triethyl phosphite) over a period of 2-5 min, using microwave-irradiation, in the presence of ZnO nanoparticles as catalyst. The obtained bioactivity results antibacterial and antifungal activity were further validated by DFT, ADMET, pharmacokinetics and molecular docking studies.

2. Materials and methods

2.1. General information

A catalytic quantity of 5% ZnO nanoparticles was introduced into an uncovered glass tube containing a mixture of 4-methylaminophenol (6.99 mmol), triethyl phosphite (8.99 mmol), and the corresponding aldehyde (8.01 mmol). The reaction mixture was subjected to microwave as gifted source of heating to transfer the heat to the reaction mixture directly, resulting in saving time and energy required for the completion of the process between 2 and 5 min under 250 Hz as frequency using EtOH as solvent. After completion of the reaction, as indicated by TLC, silica gel dichloromethane - methanol (99/1), a mixture of diethyl ether and n-hexane (4/1) was added and the mixture was cooled to 6 °C overnight. The precipitate was filtered and dried to obtain the final product.

2.2. X-ray measurements

A single crystal of the studied compound 3e (Fig. 3) was selected for X-ray diffraction analysis. Data collection was performed, at 293(2) K, on an Agilent SUPER NOVA diffractometer, CCD area detector (ATLAS2) equipped with a mirror monochromatized Cu Kα radiation (λ= 1.54,184 Å). The crystallographic data and experimental details for structural analysis are summarized in (Table 1).The reported structures were solved by direct methods with SIR2002 [14] to locate all the non-H atoms which were refined anisotropically with SHELXL97 [15] using full matrix least squares on F^2 procedure from within the WinGX [16] suite of software used to prepare material for publication. All the H atoms were located in difference Fourier maps and were placed in the calculated positions and constrained to ride on their parent atoms. Drawings of molecules were produced with the program ORTEP-3 and Diamond [17].

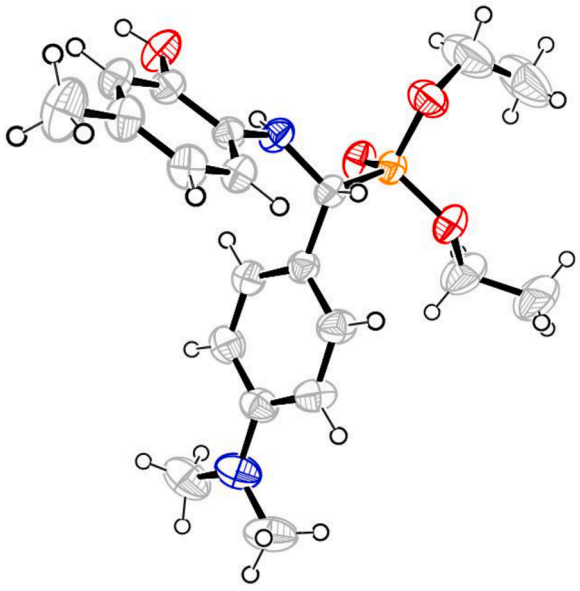

Fig. 3. Ortep diagram of compound 3e displacement ellipsoids are drawn at the 50% probability level. H atoms are represented as small spheres of arbitrary radius.

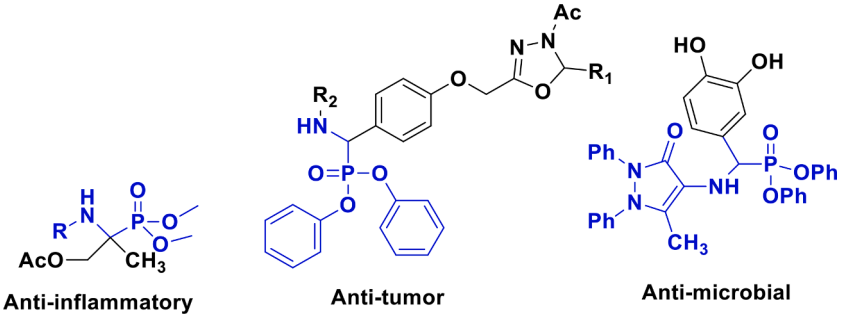

Fig. 2. Biologically active α –aminophosphonates.

Table 1
Physical characterization details of α-aminophosphonates Synthesis 3a-3 h.

Entry	Compound	Time (min)	Yields (%)	Melting point (°C)
3a	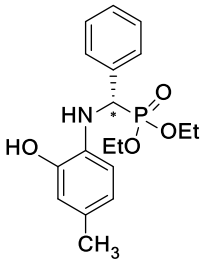	2	88	111–123
3b	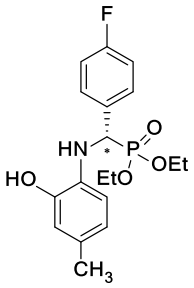	2	82	140–149
3c	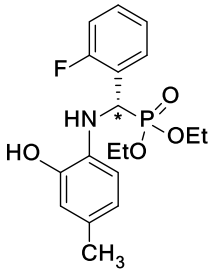	3	83	121–129
3d	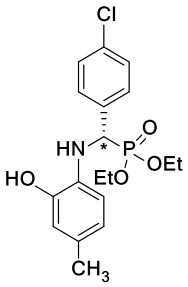	3	90	131–138
3e	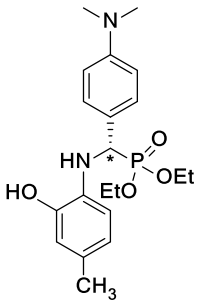	5	93	142–148

Table 1 (*continued*)

Entry	Compound	Time (min)	Yields (%)	Melting point (°C)
3f	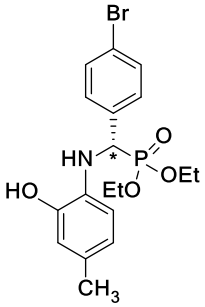	3	85	123–124
3 g	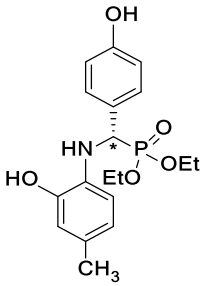	4	52	130–145
3h	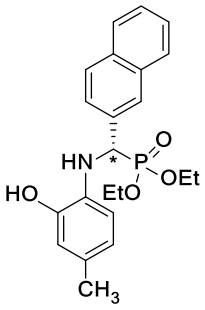	4	85	127–128

2.3. Biological activity

2.3.1. Antimicrobial activity

The antimicrobial evaluation of the chemical compounds was tested individually against a panel of Gram-negative pathogenic bacteria such as: *Escherichia coli, Klebsiella Psneumoniae, Acinetobacter baumannii, Serratia marcescens, Morganella morganii, Peudomonas aeruginosa and* Gram-positive: *Staphylococcus aureus.* And against fungi: *Candida albicans, Candida krusei, Candida kefyr, Candida lusitaniae, and Candida tropicalis.*

The agar well diffusion method was used [18]. The compounds were tested at a concentration of 5 mg/mL against bacterial and fungal strains. The microbial suspension was prepared in sterilized saline equivalent to McFarland's standard 0.5 solutions (1.5×105 cfu mL^{-1}), and its turbidity was adjusted to an optical density (OD) = 0.08 using a spectrophotometer at 600 nm.

The agar surface was swabbed and then dried for 15 min with the cover in place. Wells of 6 mm diameter were made in the solidified medium using sterile beads. The solution of the test compound (100 µL) was added to each well using a micropipette. Experimental controls include DMSO, antibiotic (amoxicillin clavulanic acid (AMC)) / antifungus (amphotericin-B) impregnated discs. The cultures were then incubated overnight at 37 °C. The absence of microbial growth showed a clear halo around the disk, then the diameters of the zone of inhibition (DZI) were measured. The results obtained were expressed using the following references: resistant interaction of the microorganism if the diameter was ⟨ 6 mm, intermediate interaction of the microorganism if the diameter was from 6 mm to 13 mm, and sensitive interaction of the microorganism if the diameter was ⟩ 13 mm.

2.3.2. Determination of the minimum inhibitory concentration (MIC)

Evaluation of antimicrobial activity by MIC determination was

performed by the solid state spot technique according to with modifications.

Stock solutions of the test compounds, as well as amoxicillin clavulanic acid and amphotericin b, were prepared in DMSO at a concentration of 1000 μg/mL and then serially diluted twice to concentrations of (500, 250.125, 62.5, and 31.25 μg/mL). Each concentration was mixed with sterile Sabouraud (Oxoid) agar in a sterile Petri dish, followed by inoculation of a defined microbial inoculum onto the agar surface. Plates were incubated at 37 °C in a microbiological oven, and MIC results were read after 24 h. Minimum Inhibitory Concentration: The MIC is recorded as the lowest concentration of the antimicrobial agent that completely inhibits growth under appropriate incubation conditions.

2.3.3. Inhibition of biofilm formation

The inhibition of biofilm formation was measured according to the method described by which allows the observation of microbial adhesion to an abiotic surface [19]. This test was performed on 96-well plates with the compounds, with the MIC concentrations. After incubation, the planktonic bacteria were washed with sterile saline solution and the adherent bacteria (biofilm) were stainedwith 0.1% crystal violet. The stained biofilms were solubilized with ethanol and transferred to 96-well flat-bottom plates. The reading is taken at 570 nm with a microplate reader.

The inhibition of biofilm formation was calculated by the following formula:

% inhibition = (A0 - A1)/A0 × 100 (6) where A0 is the absorbance of the negative control and A1 is the absorbance of the test molecule.

2.3.4. Molecular docking study

The starting crystal of DHPS (Dihydroptorate Synthase of Versinia pestis, PDB ID 3TZF) [20] was retrieved from the RCSB protein data bank (http://www.pdb.org) and was chosen as a target for docking study that was prepared and energetically minimized using the Protein Preparation wizard protocol of the Schrodinger Suite [21]. The studied ligands were prepared by LigPrep version 3.8 [22] to set to protonation states and the atom types, correctly. Bond orders were assigned, and hydrogen atoms were added to the structures.

The grid file for DHPS was generated using the Glide Grid Generation protocol in MAESTRO [16] version 16.8 with the bound ligands as centroids. The scaling factor for receptor van der Waals for the nonpolar atoms was set to 0.8 to allow for some plasticity. The other parameters were set as defaults. Flexible docking runs were performed with a single precision docking mode.

3. Results and discussion

3.1. Synthesis

The efficacious synthesis of novel α-aminophosphonate (3a-3 h) derivatives was accomplished utilizing ZnO nanoparticles as a catalyst under both microwave irradiation condition, as depicted in Scheme 1. The materials chosen for optimizing the reaction conditions were 4-methylaminophenol (1), benzaldehyde (2a), and diethylphosphite. The three component Kabachnik–Fields reaction was examined in ethanol, THF using 5 mol% of ZnO at 250 Hz to synthesize compounds 3 and the yields are shown in Table 1.

3.2. X-ray measurements

Single-crystal X-ray diffraction studies reveal that 3e is composed of a 2D framework. Structural resolution revealed that the asymmetric unit consists of one molecule of ((2S)-diethyl-(3-dimethylaminophenyl)-(2-hydroxy-4-methylphenyl) aminophosphonate), which crystallizes in the Monoclinic crystal system with *P* $2_1/n$ space group Table 2. The ellipsoid Plot (ORTEP) [16] illustration of one representative molecular structure of 3e is exposed in Fig. 4. The dihedral angles formed between two phenyl rings in the asymmetric unit is 86.97°

The crystal packing can be described as alternating double layers parallel to the (010) plane along the c axis Fig. 4, which are connected with N—H…O and O—H…O hydrogen bonds along the c axis Fig. 5, Table 3. In these layers, the arrangement of each molecule induces weak π–π staking intermolecular interactions. The distance centroid–centroid is 5.17950 (11) Å between phenyl rings in the packing crystal, which are oriented face to face with a long slippage value of 4.798 Å.

Table 2
Crystallographic data and refinement parameters for 3e.

Formula	$C_{20}H_{29}N_2O_4P$	Absorption coefficient (mm^{-1})	1.371
Formula weight	392.42	F(000)	840
Crystal habit, color	Prism, Colorless	Crystal size (mm)	0.24 × 0.30 × 0.38
Crystal system	Monoclinic	θ range for data collection (°)	4.417- 75.987
Space group	*P* $2_1/n$	Reflections collected	13,161
a (Å)	9.7644(1)	Independent reflections	4372
b (Å)	10.8310(1)	R_{int}	0.0209
c (Å)	20.0199(2)	Reflections with $I \geq 2\sigma(I)$	3963
α (°)	90	Number of parameters	250
β (°)	90.274(1)	Goodness-of-fit on F^2	1.056
γ (°)	90	Final R indices [$I \geq 2\sigma(I)$]	R_1=0.0557,
Volume ($Å^3$)	2117.24(4)	R indices [all data]	wR_2=0.1552
Z, Z'	4, 4	Largest difference peak and hole ($Å^{-3}$)	R_1=0.0552, wR_2=0.1609
Density (calculated, g cm^{-3})	1.231		
		CCDC deposition no.	0.424, −0.389 CCDC 2,221,672

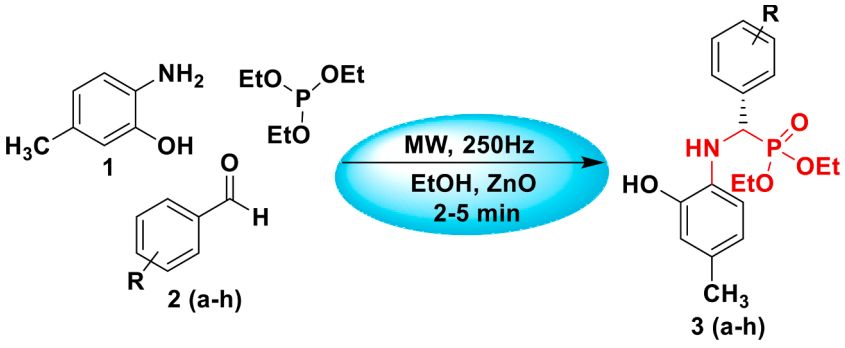

Scheme 1. Synthesis of α-aminophosphonates 3a-3 h.

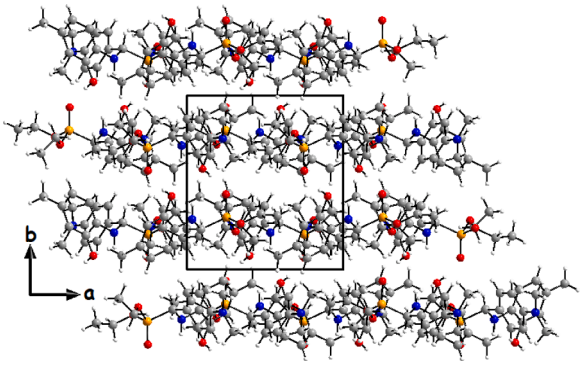

Fig. 4. Diagram packing of 3e viewed along the c axis showing double layers parallel to (010) plane along the a and c axis.

3.3. Biological activity

The newly synthesized compounds were examined for their *in vitro* antibacterial potency against bacteria: *E.coli, S.aureus, K.pneumoniae, A. baumannii, M.morgani, M.marcesens and P.aeruginosa.* They were also evaluated for their antifungal potency against Candida spices strain included: *C. albicans,C. kefyr,C.krusei,C.lusitaniae* and *C. tropicalis*. The agar-diffusion method was used to determine the preliminary antibacterial and antifungal potencies. Standard drugs such as Amoxicilin/calvunic acid were also used against bacteria, and Amphotericin b against fungal strains.

Antimicrobial results were reported: the average diameter of the zones of microbial growth inhibition around the discs are presented in Tables 4 and 5.

MIC measurements were also determined for compounds giving primary inhibition by the spot method on agar medium and the results are also reported in (Tables 6 and 7).

3.3.1. The in vitro antibactrial activity of all the synthesized

As shown in Table 4, all the synthesized compounds showed no apparent activity against *P. aeruginosa*, and *K.pneumoniae*. It is also clear that the antibacterial activity of the molecules against *A.baumannii* with inhibition diameters ranging from 12 mm to 30, and MIC ranging from 62.5 to 1000 µg/ml, compared to the action of the antibiotic Amoxicillin/clavunic acid (inhibition zone, 10 mm, MIC, 1000 µg/mL), the activity of the molecules was also interesting on the *M.morgani* strain with inhibition zone diameters ranging from 18 mm for 3a and a MIC up to 500 µg/mL . 30 mm for 3b and 3c with a MIC 62.5 µg/mL, and however 3f and 3 h showed no effect on this same species, which was also resistant to the action of the antibiotic.

S.aureus which is the only Gram-positive bacterium is sensitive to 3f and 3 h molecules with interesting diameters of 22 mm and 28 mm respectively a MIC of 500 and1000 µg/mL.

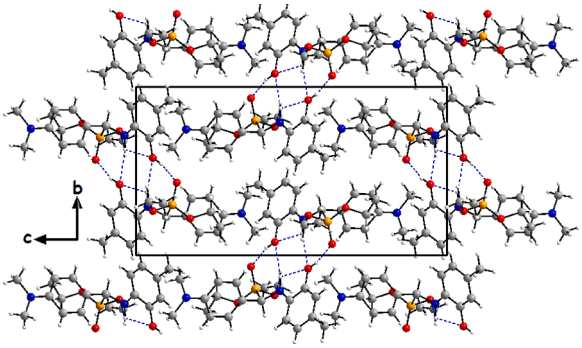

Fig. 5. Diagram packing of 3e viewed along the a axis showing N—H…O and O—H…O (dashed line in blue) hydrogen bonds interactions.

Table 3
Distances (Å) and angles (°) of hydrogen bond for 3e.

D–H…A	*d*(D–H)	*d*(H…A)	*d*(D–A)	D–H–A	Symmetry
Compound 3e					
O1-H1…O2	0.82	1.86	2.663(2)	167.0	1-x,2-y,1-z
N1-H1A…O1	0.91	2.29	2.668(2)	105.0	x,y,z
N1-H1A … O1	0.91	2.35	3.229(2)	162.0	1-x,2-y,1-z

3.3.2. The in vitro antifungal activity of all the synthesized

In vitro antifungal activity of all the synthesized compounds (3a to 3 h) was tested against five fungal strains belonging to the genus Candida, using the drug Amphotericin b as reference standard (positive control).

The results listed in Tables 5 and 7, clearly show that the tested compounds have excellent antifungal effects against the different strains tested, ranging from 10 to 50 mm diameter of inhibition zone and a MIC of 31.25 to 1000 µg/mL. With the species *C. kefyr* and *C.krusei* a total inhibition of growth is observed with the molecules 3a, 3b, 3c and 3d and 3 h. The same observation is observed with *C.lusitaniae*; and *C. tropicalis* with the molecule 3d and 3 h. The species *C. kefyr*, and *C. lusitaniae* show sensitivity towards all the tested molecules with inhibition zone diameters ranging from to with MIC, and from to with MIC of two respectively, these two species show resistance to the action of amphotericin b and based on these facts we can consider most of the synthesized compounds as potential antifungal candidates. According to the literature, the α-aminophosphonate derivatives have shown good and promising antimicrobial activity [23].

3.3.2. Biofilm assay

Biofilms are surface- or interface-attached communities of microorganisms in which cells are immersed in an exopolymeric matrix composed of polysaccharides, proteins, and DNA. More than 90% of naturally occurring microorganisms exist as biofilms [20]. Microbial biofilms are responsible for the etiology and pathogenesis of many acute and especially chronic bacterial infections in humans. Among bacterial diseases in humans and animals, more than 80% are associated with the presence of bacterial communities enclosed in biofilms [24]. The drug resistance of bacteria living in biofilms has been multiplied by several times compared to bacteria grown in plankton [20]. In this regard, the ability of pathogenic bacteria to form biofilms is an important issue. The compounds were evaluated for biofilm inhibition. Figs. 6 and 7 show that the most of the compounds inhibited biofilm formation.

The effect of the molecules on the biofilms formation by each microorganism included in our study. Crystal violet staining showed (Fig. 7) a significant inhibition of biofilm formation of bacterial and fungal clinical strains in contact with the different molecules. Interesting is to note for the different molecules a rate ranging from 11.23 to 96.39% for the inhibition of bacterial biofilm. The results were better than the test with amoxicillin/clavunic acid whose rate varied between 8.56 and 22.33%. In the case of the fungal biofilm, the effect was also very interesting with an inhibition rate ranging from 96.24 to 8.54%, largely exceeding the antibiofilm effect of amphotericin b which marked an inhibition ranging from 11.08 to 13.55%.

3.4. Molecular docking study

3.4.1. Molecular docking

Dihydropteroate synthase is an enzyme involved in the bacterial folate synthesis pathway. Where the folate synthesis pathway is a crucial pathway for synthesizing amino acids [25]. DHPS has two active sites (binding pockets): one which binds dihydropterin pyrophosphate (DHPP) and one which binds p-amino benzoic acid (pABA) [26]. (Zhao et al.), reported the amino acids residues Asp96, Asn115, Asp185, Lys221and Arg255 are essential for interaction with proterin-moeity, while, Phe190, Lys221 and Ser222 amino acids residues are crucial for interaction with pABA-moiety amino acids residues [27].

Table 4
Antibacterial activity of molecules (3a-3 h).

Bacterial Strain	3a	3b	3c	3d	3e	3f	3 g	3h	AMC	DMSO
E.coli	18	15	15	R	12	R	22	20	10	R
S.aureus	R	R	R	R	R	28	R	22	10	R
K.pneumoniae	R	R	R	R	R	R	R	R	13	R
A.baumannii	30	25	12	28	20	22	30	18	10	R
M.morgani	18	30	30	20	26	R	15	R	R	R
S.marcesens	R	18	R	R	R	R	R	15	R	R
P.aeruginosa	R	R	R	R	R	R	R	R	10	R

Table 5
Antifungal activity of the molecules.

Fungal Strain	3a	3b	3c	3d	3f	3 g	3 g	3h	Amphotericin b	DMSO
C. albicans	22	50	35	R	17	20	30	42	R	R
C. kefyr	+	+	+	+	15	20	22	+	R	R
C.krusei	+	+	+	+	20	R	R	+	20	R
C.lusitaniae	20	18	25	+	10	25	30	22	R	R
C. tropicalis	18	25	25	+	R	40	44	+	8	R

(Inhibition zone was expressed in mm).

Table 6
MIC of the Most Active Compounds against bacteria expressed in μg/ml.

Bacterial Strain	3a	3b	3c	3d	3e	3f	3 g	3h	AMC
E.coli	250	500	500	/	250	/	1000	1000	500
S.aureus	/	/	/	/	/	500	/	1000	1000
A.baumannii	125	62.5	1000	250	250	250	500	1000	1000
M.morgani	500	62.5	62.5	1000	500	/	1000	/	/
S.marcesens	/	1000	/	/	/	/	/	1000	/

Table 7
MIC of the Most Active Compounds against fungi expressed in μg/ml.

Fungal Strain	3a	3b	3c	3d	3e	3f	3 g	3h	Amphotericin b
C. albicans	250	62.5	125	/	500	500	125	1000	R
C. kefyr	31.25	31.25	31.25	31.25	62.5	1000	1000	62.5	R
C.krusei	31.25	62.5	62.5	31.25	1000	/	/	/	62.5
C.lusitaniae	1000	1000	250	31.25	1000	500	125	250	R
C. tropicalis	1000	250	250	62.5	/	31.25	31.25	31.25	125

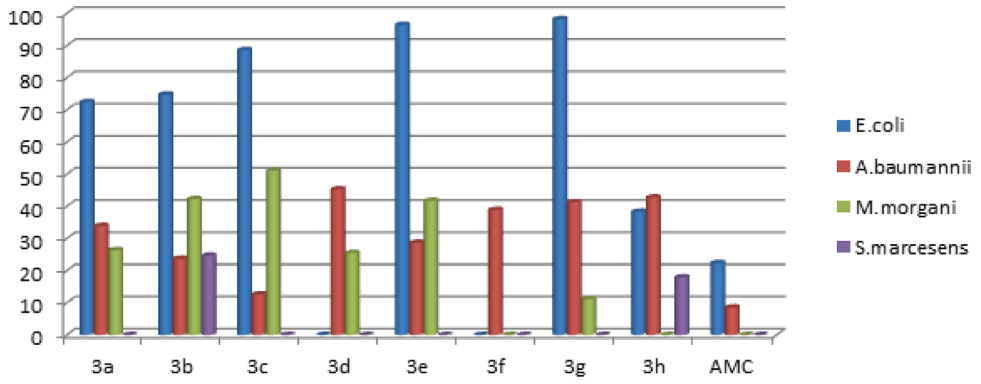

Fig. 6. Inhibition of bacterial biofilm formation by molecules.

Dihydropteroate synthase (DHPS) is the target for the sulfonamide class of antibiotics [28], therefore the aim behind this part is to explore the binding mode of studied derivatives into the binding site of DHPS using computational docking study [29]. The validation of molecular docking was done for docking methodology by re-docking the referent ligand (Sulfamethoxazole) and it was carried out successfully with RMSD <1 Å Fig. 8.

To investigate the possible mode of binding of studied compounds (3a, 3b, 3c 3d, 3e, 3f, 3 g and 3 h) to the target enzyme DHPS, we docked all of them into the target structure DHPS using Glide Grid Generation in MAESTRO. Studied ligands were ranked by docking score and binding energy of predicted poses in the binding pockets Table 8.

The molecular docking study of all compounds revealed compounds (3a, 3b, 3c, 3d, 3e, 3f, 3 g and 3 h) found to be stable inside the binding pocket and gave a better docking score and binding energy when compared with the referent ligand Table 8. We observed that all studied compounds formed 2 hydrogen bonds: one H-bond with ARG 235 residue through the oxygen atom (O_{16}) as an acceptor and one H-bond with SER 222 residue through the oxygen atom (O_{19}) of the hydroxyl group as an acceptor. Also, these compounds formed the same pi-pi interaction

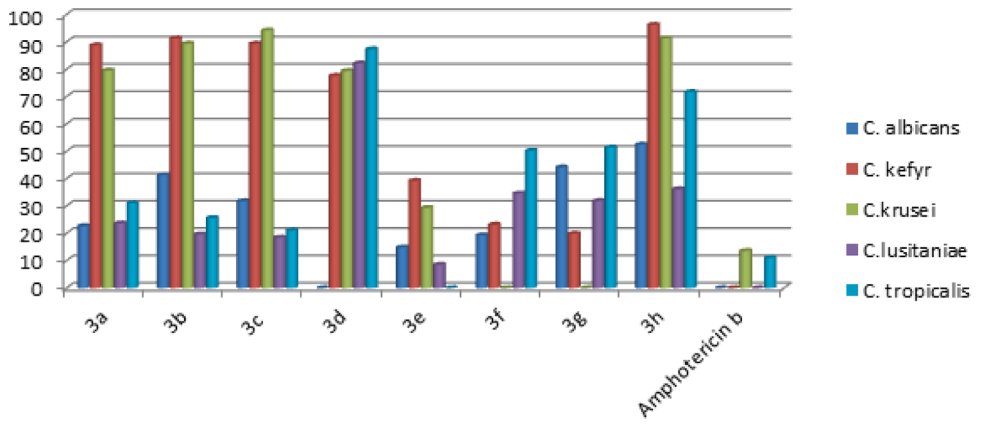

Fig. 7. Inhibition of fungical biofilm formation by molecules.

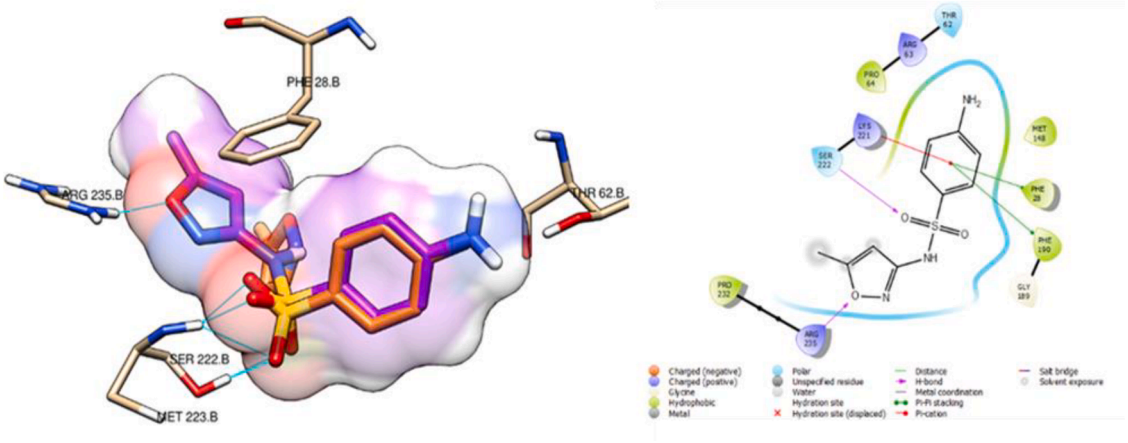

Fig. 8. Re-docking of the referent ligand (PDB id 3TZF); H-Bond interactions shown in cyan line.

between the phenyl ring of compounds and PHE 28 residue. Fig. 9 shows the superimposition of the docked compounds into the binding pocket of DHPS and Figs. 10 and 11 show the different types of interactions between ligands and the active site of DHPS. The compound 3 g is the most stable among the studied compounds which the least binding energy and a docking score Table 8 with values (of-48.828 kcal/mol), (−7.029 kcal/mol), respectively, because it formed another hydrogen bond interaction in addition to other H-bonds previously mentioned with PRO 64 residue.

Docking analysis revealed that all eight ligands interact satisfactorily with Dihydropteroate synthase DHPS, the substituents in the para position on the phenyl of ligands influenced the stability in the active site, in particular the hydroxyl group, which increased the stability as in the case of compound 3 g.

Table 8
Docking score and binding energy (kcal/mol) of studied ligands with the referent ligand.

Compound code	docking Score	Binding Energy
3a	−6.449	−45.386
3b	−6.163	−44.661
3c	−6.497	−46.078
3d	−6.188	−45.391
3e	−6.241	−46.437
3f	−6.108	−45.543
3 g	−7.029	−48.828
3h	−6.380	−47.654
co-crystalized	−6.100	−37.683

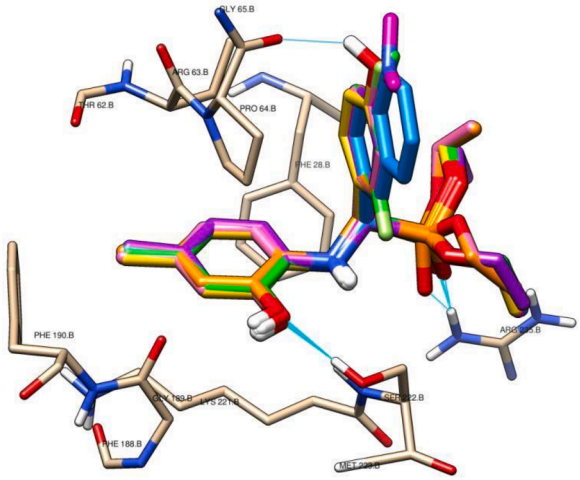

Fig. 9. superimposition of docked derivatives into DHPS; compound 3a (purple), compound 3b (pink), compound 3c (green), compound 3d (orange), compound 3e (magenta), compound 3f (brown), compound 3 g (yellow) and compound 3 g (blue). H-Bond interactions shown in cyan line.

3.5. Pharmacokinetic properties

To possess pharmacological potential and effective drug activity, a molecule must exhibit desirable pharmacokinetic properties within biological systems. Consequently, in order to investigate the

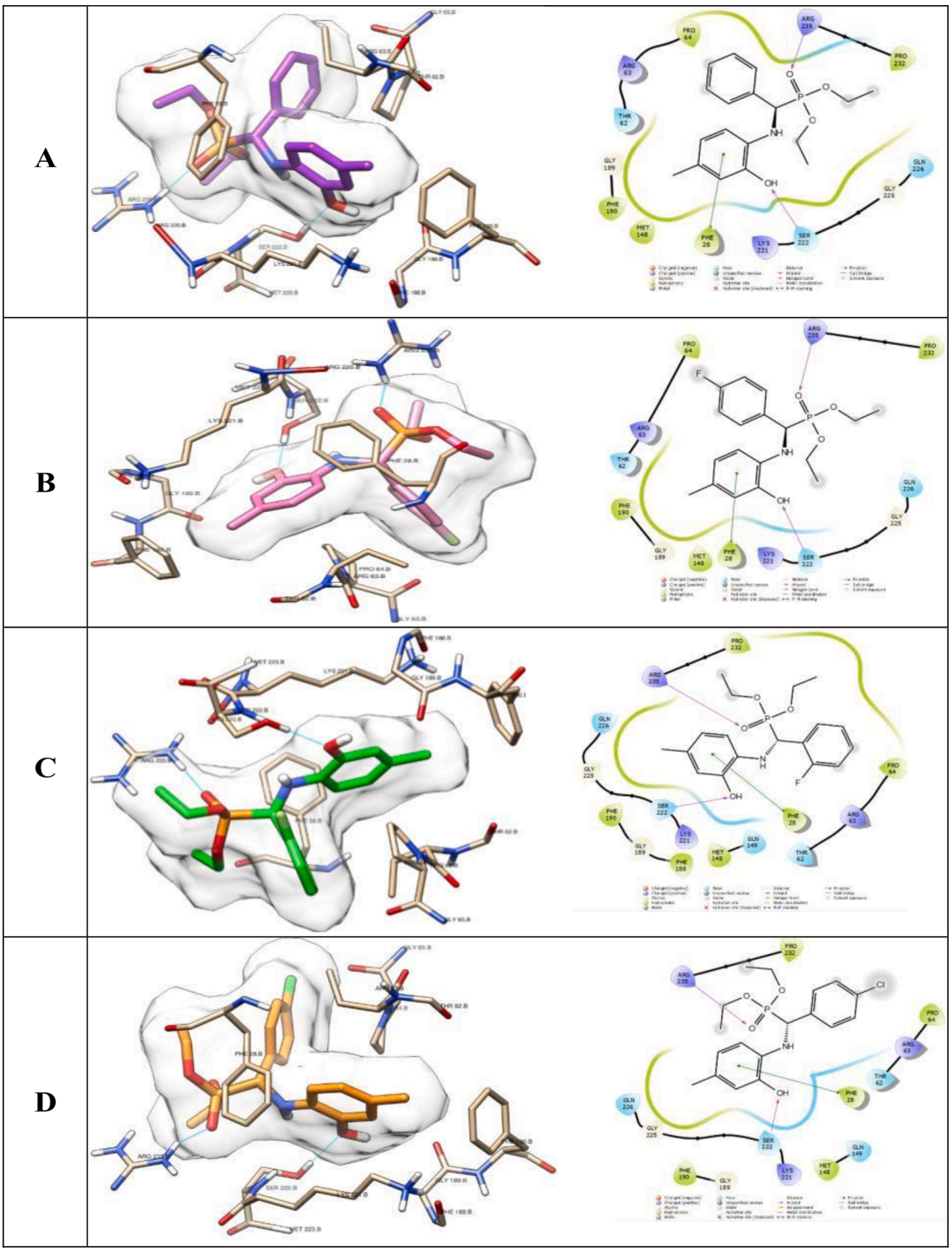

Fig. 10. 3D and 2D Docking pose of docked derivatives into DHPS; A: compound 3a (purple), B: compound 3b (pink), C: compound 3c (green) and D: compound 3d (orange). H-Bond interactions shown in cyan line.

pharmacokinetics of the synthesized molecules, we conducted a computational study utilizing Osiris and Molinspiration [30–35]. The theoretical toxicity risk evaluation for the 3a-3 h series utilizing the Osiris program indicated that all compounds exhibited lower toxicity levels than the reference clinical drug, sulfamethoxazol. Table 9.

All compounds are non-mutagenic and non-irritant. Only compound 3e is tumorigenic. Low hydrophilicities and therefore high cLogP values may cause poor absorption or permeation of inactive compounds. The reported compounds (3a-3 h) showed high-capacity DS as compared to the standard drug sulfamethoxazole Table 10.

3.6. DFT study

3.6.1. Molecular geometry

The molecular structure of a-aminophosphonates 3a-3 h is optimized using DFT at B3LYP method [36,37], with the basic set of 6–31 G (d,p) implemented the Gaussian 09 package.

The optimized molecular structure along with the numbering of

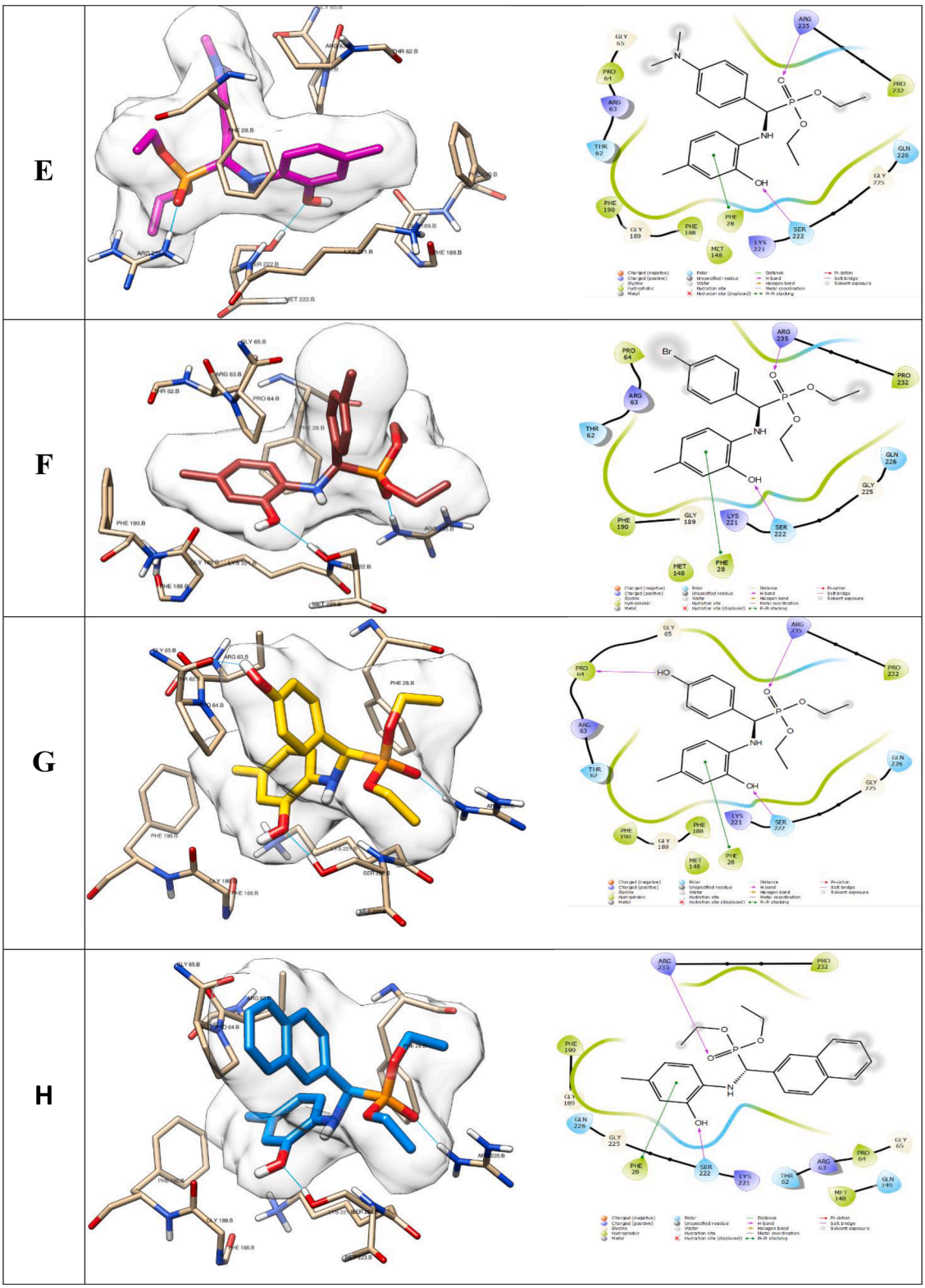

Fig. 11. 3D and 2D Docking pose of docked derivatives into DHPS; E: compound 3e (magenta), F: compound 3f (brown), G: compound 3 g (yellow) and H: compound 3 h (blue). H-Bond interactions shown in cyan line.

atoms of the title compound is shown in Fig. 12.

3.6.2. Frontier molecular orbitals (FMOs) analysis and global reactivity descriptors

FMOs analysis is a reliable method for identifying the molecular reactivity, electronic properties, and molecular transitions of a given molecule [38]. Furthermore, FMOs analysis provides valuable information regarding the properties of molecules and their interactions with biological receptors [39]. The highest occupied molecular orbital (HOMO) and lowest unoccupied molecular orbital (LUMO) are frontier molecular orbitals that are crucial in determining the chemical stability of the molecule [40]. The frontier molecular orbitals, alongside their

Table 9
Osiris calculations of toxicity risks of compounds (1a-1 h) and sulfamethoxazole.

Compdounds	MW	Toxicity Risks [a]				Osiris calculations [b]			
		MUT	TUM	IRRI	REP	cLog*P*	cLog*S*	DL	DS
3a	349					3.26	−3.64	−35.51	0.39
3b	367					3.36	−3.95	−36.23	0.37
3c	367					3.36	−3.95	−36.90	0.37
3d	383					3.86	−4.37	−34.4	0.33
3e	392					3.15	−3.57	−36.1	0.22
3f	427					3.98	−4.47	−37.5	0.3
3 g	365					2.91	−3.34	−35.26	0.4
3h	399					4.45	−5.24	−38.1	0.26
Sulfamethoxazole	253					0.44	−3.01	2.77	0.88

Higly toxic: ( ), Slightly toxic: ( ), Not toxic ( ).
[a] MUT: Mutagenic, TUM: Tumorigenic, IRRIT: Irritant, RE: Reproductive effective. [b] Sol: Solubility, DL: Druglikness, DS: Drug-Score.

Table 10
Molinspiration calculations of compounds (3a-3 h) and sulfamethoxazole.

Compdounds	Molinspiration calculations[a]				Drug-likeness [b]					
	TPSA	NONH	NV	VOL	GPCRL	ICM	KI	NRL	PI	EI
3a	68	2	0	322	−0.44	−0.12	−0.40	−0.45	−0.09	−0.08
3b	68	2	0	327	−0.41	−0.13	−0.36	−0.41	−0.10	−0.10
3c	68	2	0	327	−0.34	−0.12	−0.29	−0.35	−0.11	−0.09
3d	68	2	0	384	−0.43	−0.12	−0.41	−0.45	−0.12	−0.11
3[e]	71	2	0	368	−0.38	−0.12	−0.33	−0.38	−0.09	−0.08
3f	88	3	0	330	−0.40	−0.10	−0.37	−0.37	−0.07	−0.07
3 g	68	2	0	340	−0.52	−0.19	−0.43	−0.54	−0.19	−0.15
3h	68	2	0	366	−0.34	−0.09	−0.32	−0.35	−0.04	−0.04
Sulfamethoxazole	58	0	0	243	0.40	0.33	0.09	−0.12	−0.08	0.66

[a] TPSA: Total Molecular Polar Surface Area; NONH: number of OH—N or O—NH interaction, NV: number of violation of five Lipinsky rules; VOL: volume. [b] GPCRL: GPCR ligand; ICM: Ion Channel Modulator; KI: Kinase Inhibitor; NRL: Nuclear Receptor Ligand; PI: Protease Inhibitor; EI: Enzyme Inhibitor.

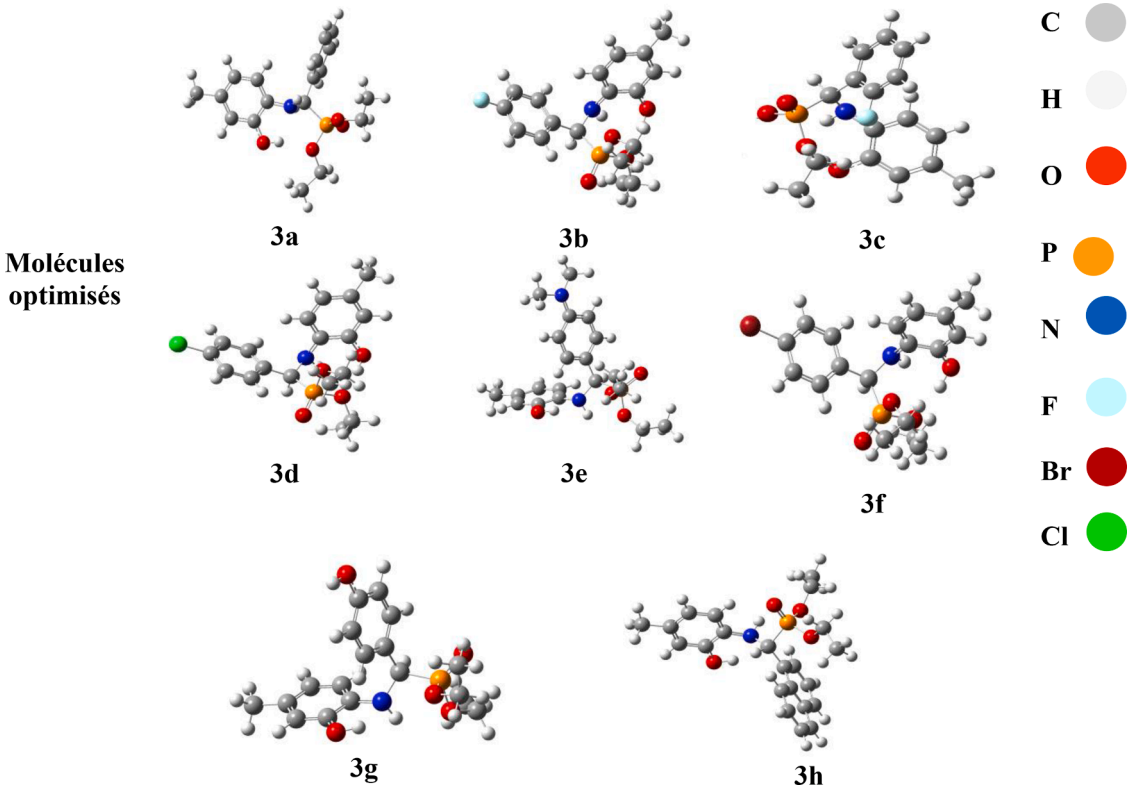

Fig. 12. The ball-and-stick model of optimized structure of α-aminophosphonates derivatives (3a-3 h) with atom numbering scheme.

corresponding energy gaps and chemical reactivity descriptors, were computed using the DFT/B3LYP/6-31 G (d,p) methodology. The calculated values have been provided in Table 11. Moreover, a molecule characterized by a lower energy gap is deemed soft, while a molecule with a higher energy gap is regarded as hard. The highest occupied molecular orbital (HOMO) and lowest unoccupied molecular orbital (LUMO) of a molecule signify its capacity to donate an electron to unfilled orbitals and its propensity to accept an electron from occupied orbitals, respectively. The energies of HOMO and LUMO, alongside the band gap of the investigated compounds, have been illustrated in Fig. 13.

Furthermore, Table 11 provides a comprehensive list of FMO-derived molecular properties, including ionization potential, electron affinity, global hardness, chemical potential, electrophilicity index, as well as hardness and softness values associated with the molecule.

The energy gap value of a molecule can be calculated using the energy difference between the HOMO and LUMO of the molecule, which explains the kinetic stability and chemical reactivity of a molecule.

In the present investigations, the energy gap of compound 3 h is 4.391 eV. A small energy gap of HOMO-LUMO means more chemical activity and low kinetic stability. The other parameters like chemical potential (μ), global hardness (η), global softness (S), electro negativity (χ), and electrophilicity index (ω) of the title molecule are computed by using HOMO and LUMO energy values.

3.6.3. Molecular electrostatic potential (MEP) analysis

The molecular electrostatic potential explores the charge distribution and polarization along with the hydrogen bonding capability and the reactivity of the molecular system. The MEP also elucidates the complete information of the electrophilic and nucleophilic sites in the molecular system, thereby providing statistical polarity of the molecule in a pictorial form, torecognize the polar and non-polar sites of the molecule in color variations as shown in the Fig. 13. The red color characterizes electrophilic reactivity (most negative), blue color characterizes nucleophilic reactivity (most positive) and green color generally illustrates nonreactive sites (zero electrostatic potential). MEP decreases in the order; blue > green > yellow > orange > red [41–42]. From the MEP plots it was concluded that amine group of α-aminophosphonate derivative possessed high electropositive potential (red) and the activated double bond of phenyl group possessed slightly low electropositive region (blue). Consequently, the phosphonate groupe of compounds (3a-3 h) support electrophilicity while the activated ethoxy group promotes nucleophilicity.

3.7. ADME predictions

The application of ADME, which refers to the absorption, distribution, metabolism, and excretion of a compound, has assumed a critical function in the drug discovery process by enabling the rational selection and optimization of lead compounds [43–44]. it represents a crucial aspect of drug development as it serves to identify prospective compounds in the early stages and mitigate the potential for deleterious effects during clinical trials by optimizing drug properties, such as absorption, distribution, metabolism, and excretion. Poor properties imply a high risk of failure for this candidate, which may become a less than ideal drug. The ADME of an ideal drug is as follows: Hydrogen bond donor, ≤5; hydrogen bond receptor, <10; molecular weight, <500 Da, lipid water partition coefficient, <5; water solubility partition coefficient, $-6.5<\log S<-0.5$ [45]. Table 12 depicts the ADME outcomes of compounds 3a-3 h, wherein the compounds satisfying the requisite criteria are deemed to possess propitious drug characteristics. Moreover, the toxicity prediction evaluation of molecules 3a-3 h unveiled that all compounds exhibited toxicity profiles conducive to drug development.

The compounds bioavailability profile was expeditiously assessed via the bioavailability radar, which incorporates six physicochemical parameters: Lipophilicity (XLOGP3 within the range of −0.7 to +5.0), Size (molecular weight ranging from 150 to 500 g/mol), Polarity (total polar surface area between 20 and 130 Å2), Solubility (log S not surpassing a certain threshold), Saturation, and Flexibility (number of rotatable bonds not exceeding a specific value).

Fig. 14 showed the physicochemical properties of α-aminophosphonates and had FLEX values that were outside the desired range for increased bioavailability.

4. Conclusion

In conclusion, in the present work, we report the synthesis, crystallographic, biological, and computational studies of the new α-aminophosphonates. The target compounds were obtained by a simple and efficient multicomponent Kabachnik-Field reaction from 4-methylaminophenol, various aldehydes and triethylphosphite. The structures of the newly synthesized compounds were determined based on usual spectroscopic data (IR, ^{1}HNMR , ^{13}CNMR). In addition, an X-ray diffraction analysis was performed on the single crystals of compound 3e further confirms the structure of the target molecules. All compounds were evaluated for their antibacterial and antifungal activities. The tested compounds have excellent antifungal effects against the different strains tested, ranging from 10 to 50 mm diameter of inhibition zone a MIC of 31.25 to 1000 μg/mL. In addition, a docking study was performed on targeted compounds to support the experimental results, and showed high docking score and good binding energy with the target enzyme. Higher docking scores and binding free energies were observed for the investigated compounds compared to the reference ligand.

CRediT authorship contribution statement

Rania Bahadi and Rayenne Redjemia: Synthesis of molecules; **Chahrazed Benzaid and Manel Lina Djendi:** Biological evaluation; **Ali**

Table 11
Calculated EHOMO, ELUMO, EGAP, absolute softness (*σ*), absolute hardness (*η*), optical softness (*σ0*), chemical potential (*CP*), absolute electronegativity (*χ*), additional electronic charges (*ΔNmax*) nucleophilicity index (*N*) and electrophilicity index (*ω*) for all the synthesized compounds 3a-3 h at DFT/B3LYP/6–31G(d,p) level.

Molecular Descriptors	Gaz phase							
	3a	3b	3c	3d	3e	3f	3 g	3h
Log P	4.65	4.54	4.54	4.92	4.67	5.19	4.12	5.65
α_{Tot}	223.43	222.19	222.20	235.35	258.73	243.49	225.62	268.52
μ (D)	2.365	3.005	0.744	3.653	1.839	3.542	1.565	4.126
E_{HOMO}	−5.529	−5.384	−5.299	−5.437	−5.085	−5.430	−5.676	−5.516
E_{LUMO}	−0.293	−0.281	−0.584	−0.469	−0.009	−0.488	−0.140	−1.125
ΔEgap	5.036	5.103	4.715	4.968	5.076	4.942	5.536	4.391
E (u.a)	−1397.434	−1496.658	−1496.661	−1857.021	−1531.401	−3968.530	−1472.647	−1551.072
(η)	2.498	2.551	2.357	2.484	2.538	2.471	2.768	2.195
(*S*)	0.405	0.392	0.424	0.403	0.394	0.404	0.361	0.455
(μ)	−2.911	−2.832	−2.941	−2.953	−2.547	−2.959	−2.908	−3.320
(χ)	2.911	2.832	2.941	2.953	2.547	2.959	2.908	3.320
(ω)	1.696	1.572	1.835	1.755	1.278	1.772	1.527	2.511

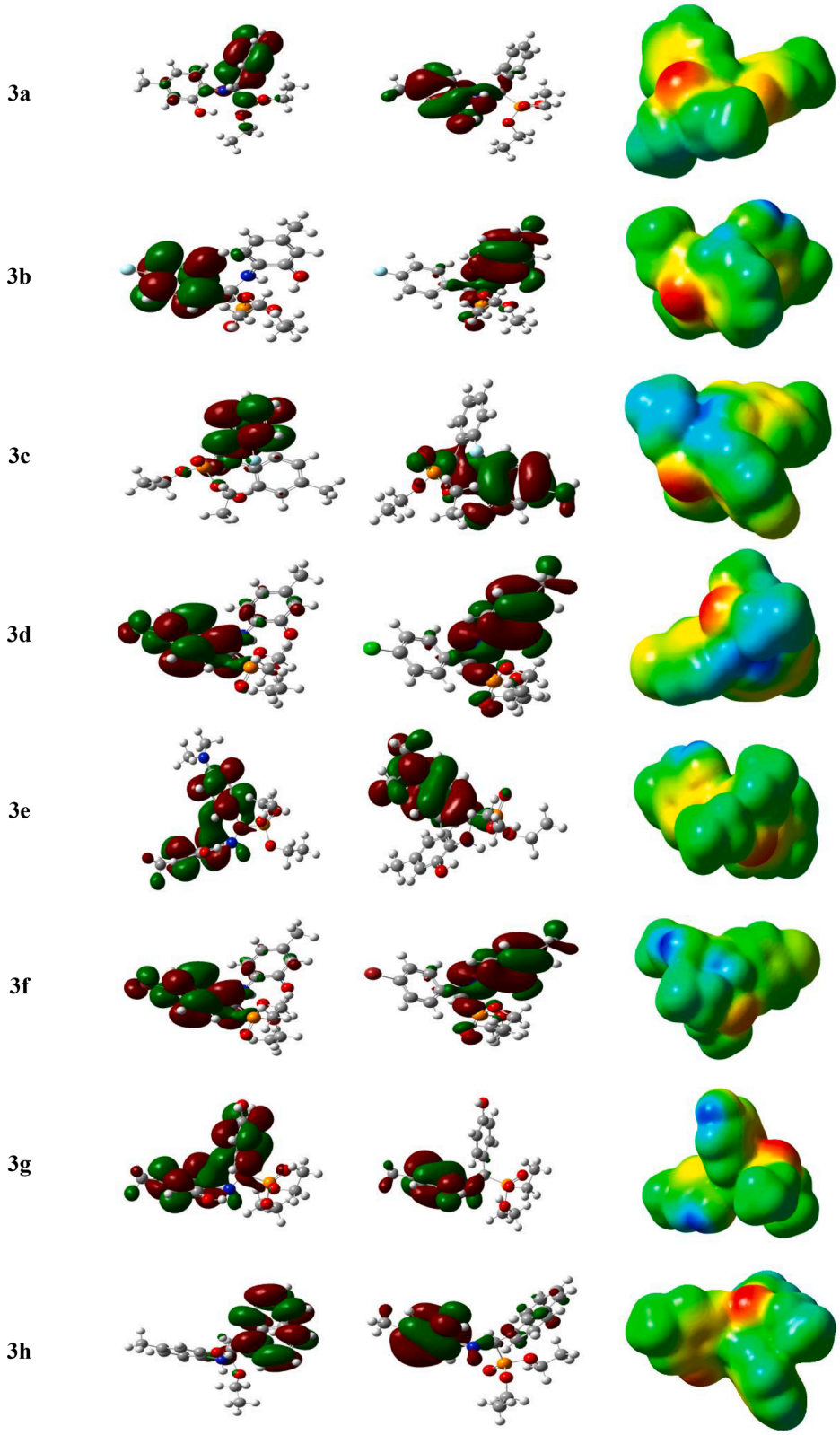

Fig. 13. HOMO, LUMO and MEPS for all the synthesized compounds (3a-3 h) at B3LYP/6–31 G (d, p) level.

Dekir and Sumeer Ahmed: Molecular docking; **Ajmal Rashid Bhat, Meriem Boussaker and Fouzia Bouchareb:** DFT and ADMET study; **Khaldoun Bachari:** Spectral analysis; **Sofiane Bouacida and Malika Ibrahim-Ouali:** Crystallographic Study; **Malika Berredjem:** Conceptualization, Methodology, Writing- Reviewing and Editing Software.

Declaration of Competing Interest

The authors declare that they have no known competing financial interests or personal relationships that could have appeared to influence the work reported in this paper.

Table 12
Interpretation of drugability violation of α-aminophosphonates.

	Molecular weight (g/mole)	Rotatable bonds	H-bond donor	H-bond acceptor	Violation LIPINSKI	Log Po/W iLogP	Log S ESOL	GI	BBB	Log Kp cm/s	Bioavailability Score
3a	349.39	8	2	4	0	3.06	−4.04	High	No	−5.93	0.55
3b	367.35	8	2	5	0	3.41	−4.23	High	Yes	−5.97	0.55
3c	367.35	8	2	5	0	3.33	−4.32	High	No	−5.97	0.55
3d	381.83	8	2	4	0	3.52	−4.66	High	No	−4.66	0.55
3e	392.43	9	2	4	0	3.39	−4.30	High	No	−6.11	0.55
3f	428.26	8	2	4	0	3.45	−4.97	High	No	−5.92	0.55
3 g	365.36	8	3	5	0	2.52	−4.90	High	No	−6.28	0.55
3h	399.42	8	2	4	0	3.51	−5.22	High	No	−5.35	0.55
CHP	350.59	6	0	4	0	3.18	−4.99	High	No	−4.92	0.55

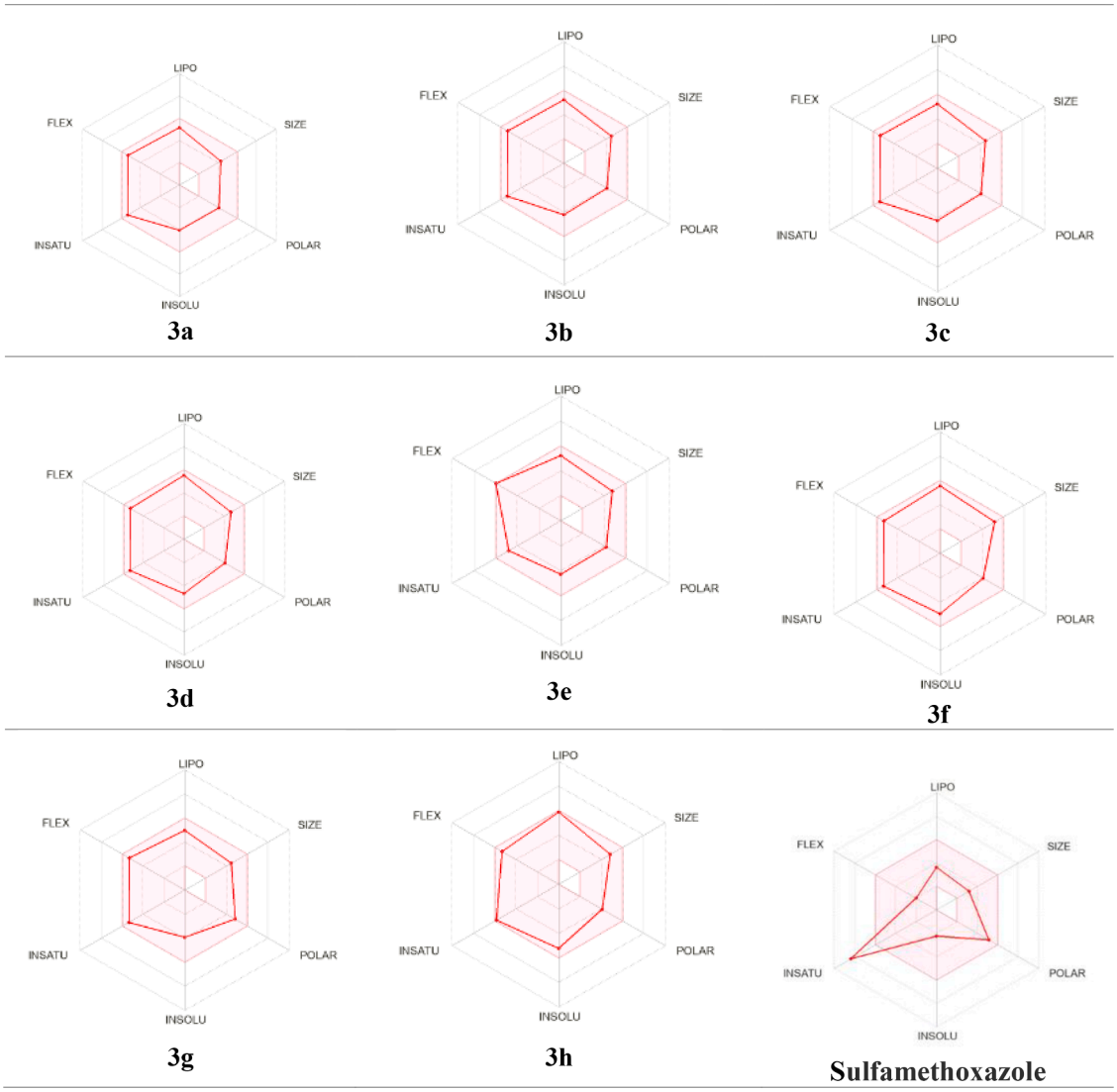

Fig. 14. Radar related to physicochemical properties of compounds α-aminophosphonates.

Data availability

No data was used for the research described in the article.

Acknowledgements

This work was supported financially by The General Directorate for Scientific Research and Technological Development (DG-RSDT), Algerian Ministry of Scientific Research, Applied Organic Chemistry Laboratory (FNR 2000).

Supplementary materials

Supplementary material associated with this article can be found, in the online version, at doi:10.1016/j.molstruc.2023.135849.

References

[1] (a) E. Breuer, F.R. Heartly, Acylphosphonates and their derivatives. The Chemistry of Organophosphorus Compounds, John Wiley and Sons, New York, 1996, pp. 653–729;
(b) F. Bouchareb, M. Berredjem, Recent progress in the synthesis of phosphoramidate and phosphonamide derivatives: a review, phosphorus, sulfur and silicon Relat, Element 197 (2022) 711–731, https://doi.org/10.1080/10426507.2021.2012781;
(c) R. Bahadi, M. Berredjem, R. Bouasla, B. Belhani, F. Bouchareb, M. Boussaker, R. Redjemia, Recent progress in synthesis of oxazaphosphinanes and their biological applications: a review, phosphorus, sulfur and silicon Relat, Element 198 (2023) 1–9, https://doi.org/10.1080/10426507.2022.2114477.

[2] (a) P. Sreelakshmi, R.N. Maheshwara, S. Santhisudha, G. Mohan, N. Saichaithanya, M.S. Shaik, P. Kotha, N. Chamarthi, S.R. Cirandur, Nano Sb_2O_3 catalyzed green synthesis, cytotoxic activity, and molecular docking study of novel α-aminophosphonates, Med. Chem. Res. 28 (2019) 528–544, https://doi.org/10.1007/s00044-019-02302-y;
(b) H. El Boraey, A.A. El Gokha, I. El Saye, Transition metal complexes of α-aminophosphonates part I: synthesis, spectroscopic characterization, and *in vitro* anticancer activity of copper (II) complexes of α-aminophosphonates, Med. Chem. Res. 24 (2014) 2142–2153. https://www.researchgate.net/publication/276427499.

[3] A.A. El Gokha, A.A.S. Ahmed, N.A.M. Abdelwahed, I.E.T. El Sayed, Synthesis and antimicrobial activity of novel mono- and bis-α-aminophosphonate derivatives, Int. J. Pharm. Sci. Rev. Res. 36 (2016) 35–39.

[4] A. Saikiran, V.N. Badavath, G. Mohan, S. Murali, R.N. Bakthavatchala, B. R. Nemallapudi, G. Sravya, V.Z. Grigoriy, R.C. Naga, R.C. Suresh, Novel α-Aminophosphonates of imatinib Intermediate: synthesis, anticancer Activity, human Abl tyrosine kinase Inhibition, ADME and toxicity prediction, Bioorg. Chem. 109 (2019), 104718, https://doi.org/10.1016/j.bioorg.2021.104718.

[5] D. Elsherbiny, M.A. Abdelrahman, E. Mehrez, A. Ramy, M.H. El-Sherbiny, I. El-Rafie, E.S. El-Tantawy, Synthesis, antimicrobial activity, and sustainable release of novel α-aminophosphonate derivatives loaded carrageenan cryogel, Int. J. Biol. Macromol. 163 (2020) 69–107, https://doi.org/10.1016/j.ijbiomac.2020.06.251.

[6] Y. Xu, K. Yan, B. Song, G. Xu, S. Yang, W. Xue, H. Deyu, P. Lu, G. Ouyang, L. Jin, Z. Chen, Synthesis and antiviral bioactivities of α-aminophosphonates containing alkoxyethyl moieties, Molecules 11 (2006) 666–676, https://doi.org/10.3390/11090666.

[7] L. Maier, P.J. Diel, Synthesis, physical and biological properties of the phosphorus analogues of phenylalanine and related compounds, Phosphorus Sulfur Silicon Relat. Elem. 9 (1994) 259–279, https://doi.org/10.1080/10426509408016410.

[8] P. Kafarski, B. Lejczak, Biological activity of aminophosphonic acids, Phosphorus Sulfur Silicon Relat. Elem. 63 (1991) 193–215, https://doi.org/10.1080/10426509108029443.

[9] K.D. Treov, Chemistry and Application of H-Phosphonates, 1st, 2006.

[10] R.A. Cherkasov, V.I. Galkin, The Kabachnik–fields reaction: synthetic potential and the problem of the mechanism, Russ. Chem. Rev. 67 (1998) 857–882, https://doi.org/10.1070/RC1998v067n10ABEH000421.

[11] (a) T.A. Mastrykukova, I.M. Aladzheva, I.V. Lemonteva, P.V. Petrovski, E.I. Fedin, M.I. Kabachnik, Dyadic phosphorus-carbon tautomerism, Pure Appl. Chem. 52 (1980) 945–957, https://doi.org/10.1351/pac198052040945;
(b) G.M. Kosolapoff, L. Maier, Organic Phosphorus Compounds, John Wiley & Sons Inc, NewYork, 1973.(c) A. N. Pudovik, "Doklady Akod, Nauk, SSSR", 83 (1952) 865, Chem Abst. 47 (1953) 4300.

[12] P.G. Baraldi, A. Barco, S. Benetti, G.P. Pollini, D. Simoni, Synthesis of natural products via isoxazoles, Synthesis 10 (1987) 857–869, https://doi.org/10.1055/s-1987-28105. Mass.

[13] R. Bahadi, R. Boughoula, M. Berredjem, K. Bachari, A. Bouzina, S. Bouacida, H. Sbartai, F. Benalliouche, R. Redjemia, A convenient synthesis, biological activity and Xray crystallography of novel α-aminophosphonate derivatives, Phosphorus Sulfur Silicon Relat. Elem. 197 (2022) 1150–1156, https://doi.org/10.1080/10426507.2022.2064859.

[14] M.C. Burla, R. Caliandro, M. Camalli, B. Carrozzini, G.L. Cascarano, L. De Caro, C. Giacovazzo, G. Polidori, R. Spagna, SIR2004: an improved tool for crystal structure determination and refinement, J. Appl. Cryst. 38 (2005) 381–388.

[15] G.M. Sheldrick, A short history of SHELX, Acta Cryst. A64 (2008) 112–122, https://doi.org/10.1107/S0108767307043930.

[16] L.J. Farrugia, WinGX and ORTEP for Windows: an update, J. Appl. Cryst. 45 (2012) 849–854, https://doi.org/10.1107/S0021889812029111.

[17] K. Brandenburg, M. Berndt, Diamond. Crystal Impact, 2001. Bonn(Version 2.1).

[18] A. Dekir, M. Berredjem, C. Benzaid, S.E. Djouad, N. Iqbal, Y. Laichi, K. Bachari, A. R. Bhat, A. Bouzina, M. Aissaoui, F. Bouchareb, Novel N-acylsulfonamides: synthesis, in silicoprediction, molecular docking dynamic simulation,antimicrobial and anti-inflammatory activities, J. Biomol. Struct. Dyn. (2023), https://doi.org/10.1080/07391102.2022.2148751.

[19] C. Benzaid, A. Belmadani, R. Djeribi, M. Rouabhia, The effects of mentha × piperita essential oil on C. albicans growth, transition, biofilm formation, and the expression of secreted aspartyl proteinases genes, Antibiotics 8 (2019) 1–15, https://doi.org/10.3390/antibiotics8010010.

[20] M.K. Yun, Y. Wu, Z. Li, Y. Zhao, M.B. Waddell, A.M. Ferreira, R.E. Lee, D. Bashford, S.W. White, Catalysis and sulfa drug resistance in dihydropteroate synthase, Science 335 (2012) 1110–1114, https://doi.org/10.1126/science1214641.

[21] G.M. Sastry, M. Adzhigirey, T. Day, R. Annabhimoju, W. Sherman, Protein and ligand preparation: parameters, protocols, and influence on virtual screening enrichments, J. Comput. Aided Mol. Des. 3 (2013) 221–234, https://doi.org/10.1007/s10822-013-9644-8.

[22] Lig Prep, Schrödinger, LLC, New York, NY, 2016 version 3.8.

[23] B. Litim, Z. Cheraiet, S. Meliani, A. Djahoudi, A. Boukhari, Synthesis and potent antimicrobial activity of novel coumarylthiazole α-aminophosphonates derivatives, Mol. Divers. 26 (2021) 1161–1174, https://doi.org/10.1007/s11030-021-10242-2.

[24] A. Smolobochkin, A. Gazizov, M. Sazykina, N. Akylbekov, E. Chugunova, I. Sazykin, A. Gildebrant, J. Voronina, A. Burilov, S. Karchava, M. Klimova, A. Voloshina, A. Sapunova, E. Klimanova, T. Sashenkova, U. Allayarova, A. Balakina, D. Mishchenko, Synthesis of novel 2-(Het)arylpyrrolidine derivatives and evaluation of their anticancer and anti-biofilm activity, Molecules 24 (2019) 3086–3114, https://doi.org/10.3390/molecules24173086.

[25] J. Slock, D.P. Stahly, C. Han, E.W. Six, I.P. Crawford, An apparent Bacillus subtilis folic acid biosynthetic operon containing pab, an amphibolic trpG gene, a third gene required for synthesis of para-aminobenzoic acid, and the dihydropteroate synthase gene, J. Bacteriol. Res. 172 (1990) 7211–7226, https://doi.org/10.1128/jb.172.12.7211-7226.1990.

[26] K.E. Hevener, M. Yun, J. Qi, I.D. Kerr, K. Babaoglu, J.G. Hurdle, K. Balakrishna, S. W. White, R.E. Lee, Structural studies of pterin-based inhibitors of dihyropteroate synthase, J. Med. Chem. 53 (2010) 166–177, https://doi.org/10.1021/jm900861d.

[27] Y. Zhao, W.R. Shadrick, M.J. Wallace, Y. Wu, E.C. Griffith, J. Qi, M.-.K. Yun, S. W. White, R.E. Lee, Pterin–sulfa conjugates as dihydropteroate synthase inhibitors and antibacterial agents, Bioorg. Med. Chem. Lett. 26 (2016) 3950–3954, https://doi.org/10.1016/j.bmcl.2016.07.006.

[28] M.L. Dennis, M.D. Lee, J.R. Harjani, M. Ahmed, A.J. Debono, N.P. Pitcher, Z. C. Wang, S. Chhabra, N. Barlow, R. Rahmani, B. Cleary, O. Dolezal, M. Hattarki, L. Aurelio, J. Shonberg, B. Graham, T.S. Peat, J.B. Baell, J.D. Swarbrick, 8-Mercaptoguanine derivatives as inhibitors of dihydropteroate synthase, Chem. Eur. J. 24 (2018) 1922–1930, https://doi.org/10.1002/chem.201704730.

[29] I.D. Kuntz, Structure-based strategies for drug design and discovery, Science 5073 (1992) 1078–1082, https://doi.org/10.1126/science.257.5073.1078.

[30] K. Bechlem, M. Aissaoui, B. Belhani, K. Otmane Rachedi, S. Bouacida, R. Bahadi, S. E. Djouad, R. Ben Mansour, M. Bouaziz, F. Almalki, T. Ben Hadda, M. Berredjem, Synthesis, X-ray crystallographic study and molecular docking of new α-sulfamidophosphonates: POM analyses of their cytotoxic activity, J. Mol. Struct. 1210 (2020), 127990, https://doi.org/10.1016/j.molstruc.2020.127990.

[31] K. Otmane Rachedi, T.S. Ouk, R. Bahadi, A. Bouzina, S.E. Djouad, K. Bechlem, R. Zerrouki, T. Ben Hadda, F. Almalki, M. Berredjem, Synthesis, DFT and POM analyses of cytotoxicity activity of α-amidophosphonates derivatives: identification of potential antiviral O,O-pharmacophore site, J. Mol. Struct. 1197 (2019) 196–203, https://doi.org/10.1016/j.molstruc.2019.07.053.

[32] K.O. Rachedi, R. Bahadi, M. Aissaoui, T. Ben Hadda, B. Belhani, A. Bouzina, M. Berredjem, D.F.T. Study, POM analyses and molecular docking of novel oxazaphosphinanes: identification of antifungal pharmacophore site, Indones. J. Chem. 20 (2020) 440–450, https://doi.org/10.22146/ijc.46375.

[33] I. Grib, M. Berredjem, K. Otmane Rachedi, S.E. Djouad, S. Bouacida, R. Bahadi, T. S. Ouk, M. Kadri, T. Ben Hadda, B. Belhani, a novel N-sulfonylphthalimides: efficient synthesis, X-ray characterization, spectral investigations, POM analyses, DFT computations and antibacterial activity, J. Mol. Struct. 1217 (2020), 128423, https://doi.org/10.1016/j.molstruc.2020.128423.

[34] A.R. Bhat, R.S. Dongre, F.A. Almalki, M. Berredjem, M. Aissaoui, R. Touzani, T. Ben Hadda, M.S. Akhter, Synthesis, biological activity and POM/DFT/docking analyses of annulated pyrano[2,3-*d*]pyrimidine derivatives: identification of antibacterial and antitumor pharmacophore sites, Bioorg. Chem. (2020), 104480, https://doi.org/10.1016/j.bioorg.2020.104480.

[35] M. Rbaa, A. Hichar, P. Dohare, ElH. Anouar, Y. Lakhrissi, B. Lakhrissi, M. Berredjem, F. Almalki, V. Rastija, M. Rajabi, T. Ben Hadda, A. Zarrouk, Synthesis, characterization, biocomputational modeling and antibacterial study of novel pyran based on 8-hydroxyquinoline, A. J. Sci. Eng. 46 (2021) 5533–5542, https://doi.org/10.1007/s13369-020-05089-y.

[36] A.D. Becke, Density-functional thermochemistry. III. The role of exact exchange, J. Chem. Phys. 98 (1993) 5648–5652, https://doi.org/10.1063/1.464913.

[37] C. Lee, W. Yang, R.G. Parr, Development of the Colle-Salvetti correlation-energy formula into a functional of the electron density, Phys. Rev. B37 (1988) 785–789, https://doi.org/10.1103/PhysRevB.37.785.

[38] M.J. Frisch, G.W. Trucks, H.B. Schlegel, G.E. Scuseria, M.A. Robb, J.R. Cheeseman, G. Scalmani, V. Barone, B. Mennucci, G.A. Petersson, H. Nakatsuji, M. Caricato, X. Li, H.P. Hratchian, A.F. Izmaylov, J. Bloino, G. Zheng, J.L. Sonnenberg, M. Hada, M. Ehara, K. Toyota, R. Fukuda, J. Hasegawa, M. Ishida, T. Nakajima, Y. Honda, O. Kitao, H. Nakai, T. Vreven, J.A.M. Jr, J.E. Peralta, F. Ogliaro, M. Bearpark, J. J. Heyd, E. Brothers, K.N. Kudin, V.N. Staroverov, R. Kobayashi, J. Normand, K. Raghavachari, A. Rendell, J.C. Burant, S.S. Iyengar, J. Tomasi, M. Cossi, N. Rega, J.M. Millam, M. Klene, J.E. Knox, J.B. Cross, V. Bakken, C. Adamo, J. Jaramillo, R. Gomperts, R.E. Stratmann, O. Yazyev, A.J. Austin, R. Cammi, C. Pomelli, J. W. Ochterski, R.L. Martin, K. Morokuma, V.G. Zakrzewski, G.A. Voth, P. Salvador, J.J. Dannenberg, S. Dapprich, A.D. Daniels, Ö. Farkas, J.B. Foresman, J.V. Ortiz, J. Cioslowski, D.J. Fox, Gaussian 09, Revision A.02, 34, Gaussian Inc Wallingford CT, Wallingford CT, 2009.

[39] R.M. Asath, R. Premkumar, T. Mathavan, A.M.F. Benial, Structural, spectroscopic and molecular docking studies on 2-amino-3-chloro-5-trifluoromethyl pyridine: a potential bioactive agent, Spectrochimica Acta Part A: Mol. Biomol. Spectr. 175 (2017) 51–60, https://doi.org/10.1016/j.saa.2016.11.037.

[40] S. Premkumar, T.N. Rekha, R. Mohamed Asath, T. Mathavan, A. Milton Franklin Benial, Vibrational spectroscopic, molecular docking and density functional theory studies on 2-acetylamino-5-bromo-6-methylpyridine, Eur. J. Pharm. Sci. 82 (2016) 115–125, https://doi.org/10.1016/j.ejps.2015.11.018.

[41] A.R. Bhat, R.S. Dongre, F.A. Almalki, M. Berredjem, M. Aissaoui c, R. Touzani, T. B. Hadda, M.S. Akhter, Synthesis, biological activity and POM/DFT/docking analyses of annulated pyrano[2,3-*d*]pyrimidine derivatives: identification of antibacterial and antitumor pharmacophore sites, Bioorg. Chem. 106 (2020), 104480.

[42] T. Ben Hadda, M. Berredjem, F.A. Almalki, V. Rastija, J. Jamalis, T. Bin Emran, T. Abu-Izneid, E. Esharkawyi, L.C. Rodriguez, How to face COVID-19: proposed treatments based on remdesivir and hydroxychloroquine in the presence of zinc sulfate. Docking/DFT/POM structural analysis, J. Biomol. Struct. Dyn. 40 (2022) 9429–9442, https://doi.org/10.1080/07391102.2021.1930161.

[43] Y. Zhu, Y. Han, Y. MA, P. Yang, ADME/toxicity prediction and antitumor activity of novel nitrogenous heterocyclic compounds designed by computer targeting of alkylglycerone phosphate synthase, Oncol. Lett. 16 (2018) 1431–1438, https://doi.org/10.3892/ol.2018.8873.

[44] M.B. Battu, A.M. Chandra, D. Sriram, P. Yogeeswari, Pharmacophore-based 3DQSAR and molecular docking studies to identify new non-peptidic inhibitors of cathepsin S, Curr. Med. Chem. 21 (2014) 1910–1921, https://doi.org/10.2174/09298673113206660275.

[45] S.K. Verma, S. Thareja, Structure based comprehensive modelling, spatial fingerprints mapping and ADME screening of curcumin analogues as novel ALR2 inhibitors, PLOS One 12 (2017), e0175318, https://doi.org/10.1371/journal.pone.0175318.